Polaronic state and nanometer-scale phase separation in colossal magnetoresistive manganites

Sahana Rößler,[1] S. Ernst,[1] B. Padmanabhan,[2] Suja Elizabeth,[2] H. L. Bhat,[2] F. Steglich,[1] and S. Wirth[1]

[1]*Max Planck Institute for Chemical Physics of Solids, Nöthnitzer Straße 40, 01187 Dresden, Germany*
[2]*Department of Physics, Indian Institute of Science, Bangalore 560012, India*

(Dated: February 1, 2008)

High resolution topographic images obtained by scanning tunneling microscope in the insulating state of $Pr_{0.68}Pb_{0.32}MnO_3$ single crystals showed regular stripe-like or zigzag patterns on a width scale of 0.4–0.5 nm confirming a high temperature polaronic state. Spectroscopic studies revealed inhomogeneous maps of zero-bias conductance with small patches of metallic clusters on length scale of 2–3 nm only within a narrow temperature range close to the metal-insulator transition. The results give a direct observation of polarons in the insulating state, phase separation of nanometer-scale metallic clusters in the paramagnetic metallic state, and a homogeneous ferromagnetic state.

PACS numbers: 71.30.+h, 75.47.Lx, 68.37.Ef

There is an intense research going on to understand the remarkable and complex properties shown by a whole family of strongly correlated electron systems. In these materials, a self-inflicted, spontaneous instability of the electronic state and competing long-range interactions may result in the formation of nanometer-sized regions of different phases. Such states have been considered as charge and spin ordered stripes in under-doped cuprates [1], as polar domains in relaxor ferroelectrics [2], or as phase separation (PS) between insulating paramagnetic (pm) and conducting ferromagnetic regions [3] in mixed valence manganites of perovskite type $AMnO_3$ (A–rare earth or doped divalent ion). In the latter case, evidence for PS has been found by various experimental techniques, such as electron microscopy [4], scanning tunneling microscopy/spectroscopy (STM/S) [5, 6], magnetic force microscopy [7] and photoelectron spectroscopy [8]. These experiments showed inhomogeneities of random shape on a length scale of several hundred nanometers. Further, the PS persisted deep into the metallic state in some of these manganites. However, computational studies on models of manganites considering double exchange, Jahn-Teller (JT) interaction and long range Coulomb potential could show only regularly spaced nanometer-scale PS [9]. The random location and shape of the clusters observed experimentally [4, 5, 6, 7, 8] are conjectured to be caused by quenched disorder in the couplings induced by chemical substitution [10, 11]. Recent STS studies combined with transmission electron microscopy [12] on A-site ordered and disordered $La_{0.75}Ca_{0.25}MnO_3$ thin films showed that PS persists in the metallic state only in the disordered film. But, this study does not address the question of PS at the metal-insulator transition temperature, T_{MI}. Thus, the origin of the PS, the length scale involved, the role of quenched disorder originating from the random A-site substitution, and the temperature range at which PS occurs, remain all strongly debated.

The polaron effect due to strong JT electron-phonon coupling is considered central to understand the remark-able transport properties, specifically the colossal magnetoresistance (CMR), of manganites [13]. The high temperature polaronic state in reciprocal space has been probed experimentally [14, 15] revealing complex polaron effects such as polaron correlation, polaron ordering, and charge localization. Using STM, polarons can be imaged directly in the real space. Polaron confinement was recently observed in a layered manganite single crystal using STM [16]. Charge ordering was reported for thin films $(La_{5/8-x}Pr_x)Ca_{3/8}MnO_3$ [short range charge exchange (CE) type] in the pm state [17] and for highly doped $Bi_{0.24}Ca_{0.76}MnO_3$ single crystals [18].

Spatially resolved STS measurements [5] on thin films of $La_{0.73}Ca_{0.27}MnO_3$ on $SrTiO_3$ showed coexistence of regions with metallic, insulating as well as intermediate conductivities, extending over several hundred nanometers. However, these images were obtained at a rather high fixed bias voltage of 3 V (much larger than the semiconducting gap of 0.2–0.3 V in manganites) and may not reflect the ground state properties. On the other hand, in Ref. 6 the zero-bias conductance, $G_0 = dI/dV|_{V=0}$, of $La_{0.7}Sr_{0.3}MnO_3/MgO$ thin films was mapped as a function of temperature T, and a threshold criterion was applied to distinguish metallic and insulating regions. Such a threshold criterion will not give an unambiguous evidence for the existence of PS because any statistical distribution of conductance, whose average value shifts with T, will seem to show PS [19]. Further, in thin film samples, miss-fit strain induced by the substrates seems to influence the electrical properties [20].

To resolve some of these issues from experimental side, we carried out STM/S on $Pr_{0.68}Pb_{0.32}MnO_3$ (PPMO) single crystals providing largely strain-free materials. We address two important questions in the physics of manganites, namely, the high temperature polaronic state and the nanometer-scale electronic PS. We present STM images of polaronic Mn^{3+}-sites and doped hole localization on Mn^{4+}-sites with atomic resolution. In addition, we provide clear evidence for nanometer-scale PS and
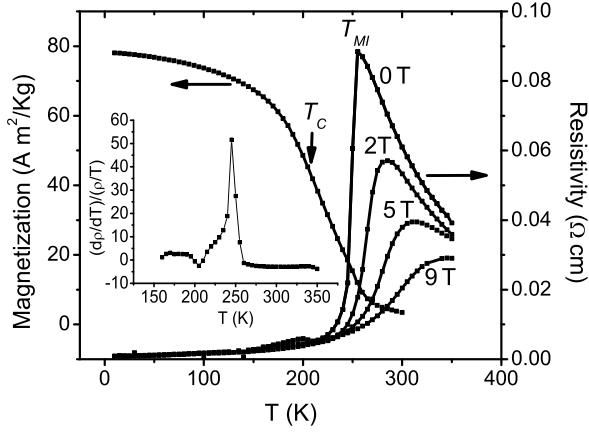
FIG. 1: Temperature dependence of magnetization (left scale) and resistivity (right scale) of $Pr_{0.68}Pb_{0.32}MnO_3$ single crystals measured at different magnetic fields. Inset: The logarithmic derivative $(d\rho/dT)/(\rho/T)$ as function of T at $H = 0$.
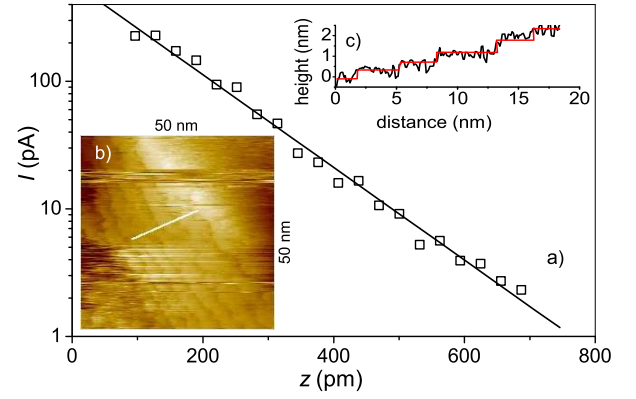

FIG. 2: (a) Dependence of tunneling current I on relative tip-sample distance z on a semi-logarithmic scale. (b) Surface topography over an area 50×50 nm^2. (c) Height profile along the white line drawn in inset (b).

percolation just below T_{MI} by looking at the entire distribution of G_0 and its dependence on T. Information on the length scale of the inhomogeneities and the T range within which it appears is obtained. We discuss the role of quenched disorder or doping and compare the results with macroscopic properties of the same single crystal.

Single crystals of PPMO used for the present study were taken from a batch of crystals, whose preparation and properties were already reported in [21, 22]. In $Pr_{1-x}Pb_xMnO_3$, the Curie temperature T_C and T_{MI} do not coincide, and metal-like conductivity occurs in a pm state in parts of the phase diagram [21, 23], a phenomenon uncommon to mixed valence manganites. Fig. 1 shows the temperature dependence of magnetization (M), resistivity (ρ) and magnetoresistive properties of a PPMO sample. The magnetoresistance, $[\rho(H) - \rho(0)]/\rho(0)$, is found to be $\sim$90% close to T_{MI} under a field of 9 T. From the maximum change in slope of the M vs. T curve, $T_C \approx 210$ K was estimated which is about 45 K lower than the corresponding $T_{MI} \approx 255$ K. Such an approach to estimate T_C is supported by elaborate investigations on a similar $Pr_{0.7}Pb_{0.3}MnO_3$ single crystal in which the so-determined $T_C \sim 197$ K agrees well with results from detailed static magnetization scaling analysis [22] as well as heat capacity measurements [24] ($T_{MI} \approx 235$ K in this compound [21]). The scaling analysis embracing the critical temperature indicated that the underlying magnetic transition is a conventional one, with short-range Heisenberg-like critical exponents. This study emphasizes on the presence of additional frustrated couplings which intercepts the formation of long range order. Deviation of the inverse susceptibility from the Curie-Weiss law above T_C [21] and history-dependent transport properties [23] suggest a presence of small magnetic metallic clusters above T_C that form percolating metallic paths upon reducing T in the pm metallic state.

Note that evidence for the formation of localized $\sim$1.2 nm magnetic clusters above T_C in another mixed valent manganite has earlier been found by small-angle neutron scattering measurements [25]. We also note the sharpness of the resistance transition which can be inferred from the logarithmic derivative of the resistance $(d\rho/dT)/(\rho/T)$ plotted in the inset of Fig. 1. Such a sharp metal-insulator transition is indicative of a strain-free sample [20] (the tolerance factor, $t = 0.965$, is close to unity indicating good ionic size match).

For the tunneling studies a STM (Omicron Nanotechnology) under ultra high vacuum conditions ($p \le 10^{-10}$ mbar) was utilized at eleven fixed temperatures, 30 K $\le T \le 300$ K, mostly in the vicinity of T_C and T_{MI}. Since crystals with perovskite structure do not cleave easily, preparation of a clean surface for the STM is a challenge. Just before inserting the crystal into the UHV chamber, we thoroughly cleaned the crystal surface in isopropanol using an ultrasonic bath and then, inside isopropanol, scraped the surface to rip off some part of the surface. This preparation gave us clean surfaces on a length scale of microns. STM was conducted using tungsten tips, and typically 0.3 nA for the current set point and 0.8 V for the bias voltage, V. This implies that we probed the unoccupied electronic DOS of PPMO. Fig. 2(a) shows the dependence of tunneling current I on relative tip-sample distance z on a semi-logarithmic plot. The exponential nature of $I(z)$ confirms an excellent vacuum tunnel barrier (effective work function $\phi \sim 1.5$ eV). Topography (50 $\times$ 50 nm^2) is presented in inset (b). Terraces with unit cell height ($\sim$0.4 nm) steps [Fig. 2, inset (c)] indicate $\langle 100 \rangle$ surface of the pseudocubic perovskite crystal.

High resolution STM images taken in the insulating regime (at 300 K) on the terraces indicate bright and dark regions forming stripe-like features spread over a length scale of 0.4–0.5 nm, as seen in Fig. 3(a), (b). While probing the unoccupied electronic DOS the doped holes
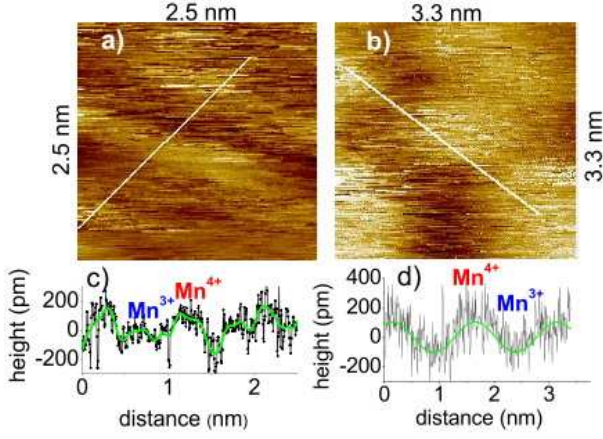
FIG. 3: (a), (b) Topography of different areas in the insulating regime ($T = 300$ K). (c) and (d) show corresponding intensity profiles along the white lines drawn in (a) and (b), respectively. The bright and dark spots in the image are associated with Mn^{4+} and Mn^{3+} ions, respectively.

localized on Mn^{4+} sites appear as bright spots in the STM image, whereas electron tunneling from a conventional metallic tip into a polaronic state (e.g. electrons localized on Mn^{3+} ions) is difficult and produces dark spots [17]. However, these contrasts were seen only occasionally, an observation similar to what was reported in the case of layered manganite $La_{2-2x}Sr_{1+2x}Mn_2O_7$ [16]. This suggests the short-range stripe-like order of Mn^{3+} and Mn^{4+} ions. The extent of these features [Fig. 3(c) and (d)] is slightly larger than the typical atomic distance of ∼0.39 nm in the cubic perovskite cell and comparable with charge ordered stripes observed in high resolution lattice images of $La_{0.33}Ca_{0.67}MnO_3$ [26]. Short-range polaron correlation and CE-type of charge ordering was observed in manganites using diffused x-ray and neutron scattering [14, 15]. Recent STM studies [17] probing simultaneously the occupied and unoccupied states of $(La_{5/8-x}Pr_x)Ca_{3/8}MnO_3$ thin films also showed short-range CE-type charge ordered clusters in the pm state.

To map the surface electronic state, we carried out thousands of STS measurements at different locations on the sample surface spanning the T range from 28 – 300 K. Typically, a surface area of 50×50 nm^2 with a lateral resolution of 1 nm (2500 pixels) was investigated. Tunneling current and differential conductance, $G = dI/dV$, were measured simultaneously while ramping V from -1 to $+1$ V. An average of 2500 G-V curves taken at representative $T = 30, 221, 260$ and 300 K are shown in Fig. 4(a). At 30 K, the G-V curve is metal-like with a finite value of G_0 signifying a finite DOS at the Fermi energy. In contrast, at 300 K, i.e. $T > T_{MI} \approx 255$ K, the G-V curve around $V = 0$ is typical of a semiconducting gap. In the pm metallic state at 221 K, the value of G_0 is only slightly reduced compared to $G_0(T = 30$ K$)$, thus showing an expected T dependence of the conductance.
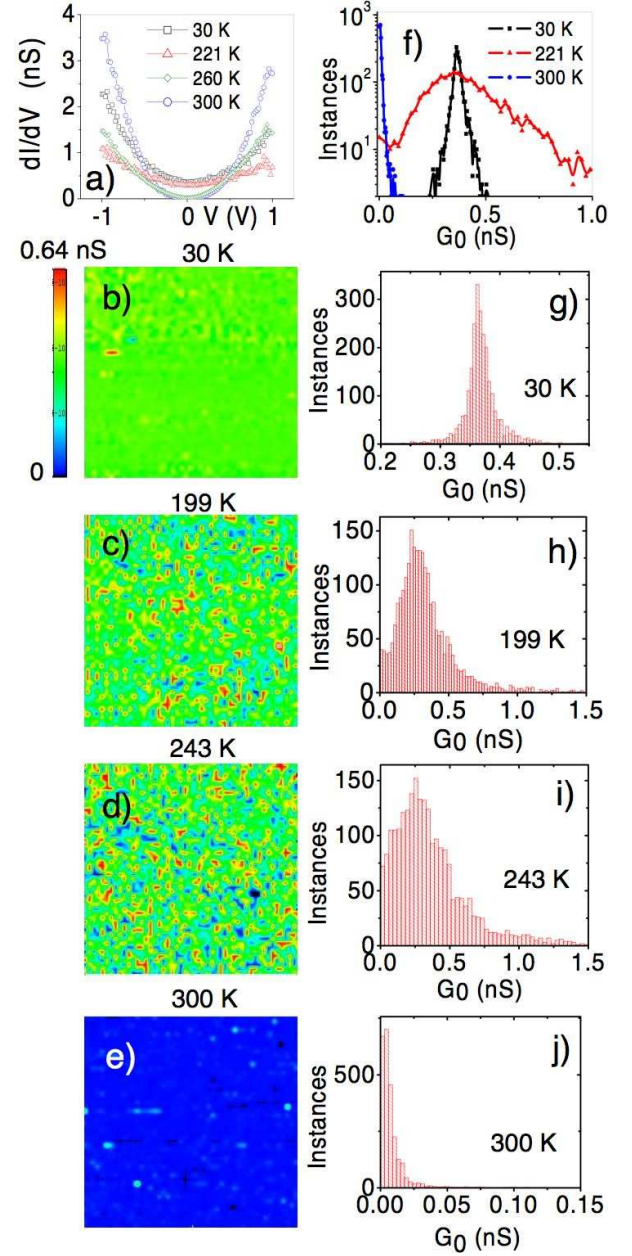
FIG. 4: (a) G-V curves averaged over an area of 50×50 nm^2 at 30, 221, 260 and 300 K indicating metallic ($T < T_{MI} \approx 255$ K) and semi-conducting behavior ($T > T_{MI}$). Panels (b)–(e) present conductance maps (50×50 nm^2) taken at 30, 199, 243 and 300 K through T_C and T_{MI}. The color scale shown left of panel (b) encodes G_0. (g)–(j) Histograms of G_0 at the same T as presented in (b)–(e). (f) Histograms for the three different T regimes compared on a semi-logarithmic scale.

For quantifying the STS results and mapping the homogeneity of the DOS laterally as well as its temperature evolution, we plot G_0 as conductance maps at selected T. In Fig. 4(b)–(e), the *local* G_0 is presented color-coded (with a color scale covering $0 \leq G_0 \leq 0.64$ nS) at $T = 30$, 199, 243 and 300 K, respectively. Corresponding distributions for the frequency of the observed G_0 values are

Rev. B **71**, 092407 (2005).

[24] B. Padmanabhan, unpublished.

[25] J. M. DeTeresa *et al.*, Nature (London) **386**, 256 (1997).

[26] S. Mori, C. H. Chen, and S. W. Cheong, Nature (London) **392**, 473 (1998).